Results in Surfaces and Interfaces 12 (2023) 100126

Contents lists available at ScienceDirect

Results in Surfaces and Interfaces

journal homepage: www.elsevier.com/locate/rsurfi

First-principles study on Boron-doped $MgF_{2-x}B_x$ (x=0.0 and 1.0) and F defected MgF_1 for anti-reflective coatings in spectacle lenses

F. Kaya Soykan [a,*], C. Soykan [b]

[a] Department of Physics, Pamukkale University, Denizli, Turkey
[b] Vocational School of Health Services, Ahi Evran University, Kırşehir, Turkey

ARTICLE INFO

Keywords:
Boron substituted magnesium fluoride
Absorption
Reflectivity
Dielectric function
Loss function

ABSTRACT

MgF_2 is ideal for anti-reflective or optical systems with light polarization. Because, it has low reflection loss, wide bandgap, high transmission efficiency. Boron is biocompatible and high strength but low density. It can be used to improve the physical properties of the MgF_2. Therefore, we have performed first-principles calculations using density functional theory (DFT) to determine the structural, mechanical, electronic, and optical properties of Boron-doped MgF_1B_1 and F-defected MgF_1 structures by modified of MgF_2 for spectacle lenses. It was determined that the elasticity and flexibility of the MgF_1B_1 phase increased compared to MgF_2. In the MgF_1 phase, the Poisson's υ ratio is larger than the other phases, so the plasticity of it is high. In addition, it is the most ductile phase since it has the lowest Pugh's (G/B) ratio of 0.264. It has moderate absorption in the 400–450 nm range. It can be used as an efficient absorber for HEV-light radiations. The light transmittance of the MgF_1B_1 phase was found to be low in the lower and upper regions of visible light and high in the middle region. It is suitable for UV filtration. For the first time, the physical, electronic, and optical properties of these phases, are reported.

1. Introduction

Magnesium fluoride (MgF_2), which is found in alkaline earth fluorides, is interesting. In particular, MgF_2 or its compounds doped using possible dopants can be used in many fields due to their good optical properties, and it is seen that they can be extremely useful in the production of lenses or coatings needed in the field of lens materials (Duyar and Durusoy, 2004). This material is ideal for optical systems where anti-reflective (AR) or light polarization is needed. Because it has low reflection loss, wide bandgap, and high transmission efficiency (Duyar and Durusoy, 2004; Kitamura et al., 2009). In addition, MgF_2 has a transparent nature over a wide spectrum range from ultraviolet to infrared. Since it will show this behavior in its dopants, it is a very good candidate for ultraviolet applications. Because the sensitivity of lens materials or coatings used in spectacle lenses to ultraviolet is very important (Korkmaz et al., 2012). The effect of ultraviolet sensitivity in the bulk production of organic spectacle lenses or the production of coatings on mineral spectacle lenses is very important in terms of protecting eye health and will greatly affect the preference for lenses or coatings. In addition, spectacle lenses are in direct contact with the atmospheric environment under normal conditions. Therefore, in case of mechanical or thermal shock (such as dropping, prolonged sunlight, welding beam, or laser beam contact) MgF_2 or its dopants are a very durable solid coating or a candidate for bulk lens materials (Kitamura et al., 2009).

When the literature is reviewed, the optical properties such as UV, Vis, and Ir, compositions, and stoichiometry of homogeneous and inhomogeneous X-ZrO_2 (X=MgF_2, SiO_2) mixed films, with X-ray diffraction and Rutherford backscattering spectroscopy (RBS) technique were investigated by R. Thiselsch and W. Meiling. In this study, it was determined that infrared absorption occurred at wavenumbers 980 cm^{-1} and 910 cm^{-1}. In addition, strong absorption of UV–Vis was observed in the MgF_2-ZrO_2 mixed films (Thielsch and Meiling, 1990). Besides, the surface structure of the MgF_2 compound was investigated by M. Wojciechowska et al. and it was determined that the MgF_2 structure could be used as an unconventional catalytic. Again in this study, the IR spectrum of the MgF_2 phase was measured. According to the data obtained, it has been observed that the absorbance value has a very high peak at wavenumbers 500–550 cm^{-1} (Wojciechowska et al., 2003). In addition, the structural, electronic, elastic, thermodynamic, and optical properties of the routine type MgF_2 crystal phase have been calculated in detail using the Density Functional Theory (DFT) by K. Ramesh Babu et al. (Babu et al., 2011). When the calculated elastic constants were analyzed, it was reported that this phase has a harder and more ductile nature than other alkali-earth fluorites. Again in this study, optical properties such as refractive index, reflection, and electron energy-loss spectrum were determined up to 30 eV photon energy

* Corresponding author.
E-mail address: fkayasoykan@gmail.com (F. Kaya Soykan).

https://doi.org/10.1016/j.rsurfi.2023.100126
Received 20 December 2022; Received in revised form 24 May 2023; Accepted 30 May 2023

range by using the calculated imaginary part of the dielectric function $\varepsilon_2(\omega)$ (Babu et al., 2011). Additionally, L.P. Wang et al. calculated the structural, electronic, and optical properties of MgF_2 (001) thin films using first-principles calculation. According to their results, it has been reported that as the layer thickness increases, the band gaps narrow, the refractive indices decrease, and the extinction coefficients increase at a small rate. It has also been reported in Wang's study that it may have anti-reflective coating properties for visible wavelengths in a certain thickness range (Wang et al., 2013). Moreover, a study of improved erosion resistance induced by Zr-oxide doping of anti-reflective TiO_2/SiO_2 coatings has recently been reported (Zambrano-Mera et al., 2023). In addition, the optical and mechanical properties of Zr-oxide-doped TiO_2/SiO_2 anti-reflective coatings for PV glass covers were investigated (Zambrano-Mera et al., 2022). Further, Zambrano et al. the mechanical and microstructural properties of broadband antireflective TiO_2/SiO_2 coatings for photovoltaic applications produced by magnetron sputtering were investigated (Zambrano-Mera et al., 2021). Finally, the physical properties of the tetragonal, orthorhombic, and cubic phases of the MgF_2 crystal structure were investigated by the FP-LMTO method using DFT (Arroussi and Ghezali, 2018).

When the previous experimental and theoretical studies we have presented above are examined, it is seen that the MgF_2 compound has good optical properties. However, optical properties can be improved by doping methods. This study aims to improve the mechanical and optical properties of MgF_2 by doping Boron into the MgF_2 crystal. But, since we are working on a material to be used in spectacle lenses, the element to be used as a dopant must be biocompatible. For this purpose, Boron was chosen as the dope element. Because, Boron is a biocompatible element as stated in the articles by A. V. Sandu et al. (Sandu et al., 2019). Besides, the ionic radius of the element Boron is smaller than the ionic radius of the element Fluorite. This is important in terms of Goldschmidt rules so that the Boron element can be placed in the MgF_2 compound (Goldschmidt, 1926). In addition, although Boron is not found in nature as an elemental, it can be obtained in high density by dissolving borate minerals in the water. Crystalline Boron, on the other hand, is a very hard element as it has a hardness of 9.5 Mohs (Helvacı, 2017). With this feature, it is aimed to improve the mechanical properties of Boron-doped $MgF_{2-x}B_x$ (x=0.0 and 1.0) and F-defected MgF_1 compounds. Furthermore, Boron compounds have a role in materials with high strength but low density. It is known that they are used against heat shock in glasses and ceramics. Due to all these effective properties, Boron was selected as a dopant in the MgF_2 compound and $MgF_{2-x}B_x$ (x=0.0 and 1.0), and F-defected MgF_1 compounds were formed. After determining that the compounds are structurally and mechanically stable, their structural properties (lattice constants, bulk modulus B (GPa)), mechanical properties (elastic constants C_{ij}(GPa), bulk modulus B (GPa), Young's modulus E (GPa), shear modulus G (GPa), Poisson's ratio ν and Pugh's ratio (G/B)), electronic properties (Density of state (DOS) and Partial density of state ($pDOS$)) and optical properties (Absorption, Dielectric function, Loss function, Reflectivity, and Refractive index) were calculated.

The most important point is that no detailed theoretical or experimental studies have been reported in the literature concerning Boron-doped $MgF_{2-x}B_x$ (x=0.0 and 1.0) and F-defected MgF_1 compounds. Therefore, the structural, mechanical, electronic, and optical properties of MgF_1B_1 and MgF_1 crystal phases formed as a result of Boron substitution and F-defected formation in the MgF_2 crystal structure are reported for the first time in this study.

2. Computational method

All total-energy calculations are performed with the CASTEP code, based on the Density Functional Theory (DFT) using the plane-wave pseudopotential method (Clark et al., 2005; Kresse and Furthmuller, 1996a,b; Kresse and Hafner, 1994). To describe the exchange–correlation function used the generalized gradient approximation (GGA) was developed by Perdew, Burke, and Enrzerhof (PBE) (Perdew et al., 1996).

Pseudopotentials were used together with an energy cutoff of 900 eV of all crystal structures for geometry optimization. For most calculations in crystals, it is sufficient to perform periodic functions of the Bloch wave vector for the entire Brillouin zone (BZ) or parts specified above it. To optimize calculations, it is useful to calculate these functions only at a carefully selected set of points in the BZ. This is even more useful in complex calculations where computational effort is important for each BZ point (Monkhorst and Pack, 1976). Therefore, Monshorst-Pack special points mesh with a size $9 \times 6 \times 3$ has been selected for all calculations. The combination of valence electrons was equivalent to Mg $2s^2$ $2p^6$ $3s^2$, F $2s^2$ $2p^5$, and B $2s^2$ $2p^1$. The convergence tolerance in all geometric optimization calculations was determined by the BFGS minimization scheme (Fischer and Almlof, 1992). It was set to *fine* quality. Thus, the energy convergence criterion of the electronic self-consistency, energy, maximum force, maximum stress, and maximum atomic displacement was used as 1.0×10^{-6} eV/atom, 1×10^{-5} eV/atom, 0.03 eV/Å, 0.05 GPa, and 0.001 Å, respectively.

Further, the elastic constants (C_{ij}) and their related properties were calculated to determine the mechanical stability and behavior of all studied phases. The electronic properties such as partial density of states ($pDOS$) were predicted for determining the effect of Boron dopant and F-defect states on electronic structures of the Boron-doped $MgF_{2-x}B_x$ (x=0.0 and 1.0) and F-defected MgF_1 compounds. Finally, the optical properties were calculated after single- point energy run utilizing norm-conserving pseudopotentials.

3. Results and discussion

3.1. Structural properties

The ground state equilibrium lattice parameters of the compounds given in Table 1 were calculated at 0 *K* and 0 *GPa*. According to our results, the MgF_2, Boron-doped MgF_1B_1, and F-defected MgF_1 phases retained their orthorhombic crystal structures after reaching structural equilibrium. The crystal structures of (a) $MgF_{2-x}B_x$ (x=0.0), (b) Boron doped $MgF_{2-x}B_x$ (x=1.0), and (c) F-defected MgF_1 compounds are illustrated in Fig. 1. In previous studies, structural properties of the MgF_2 crystal structure such as lattice constant, lattice angles, and bulk modulus have been reported (Arroussi and Ghezali, 2018; Material research, 2011; Haines et al., 2001). When the literature is examined, the densities of crystal structures in MgF_2 fluoride vary from 1.87 g/cm^3 to 3.47 g/cm^3 (Material research, 2021). As given in Table 1, when the orthorhombic *Pnnm* and *Imma 74* crystal phases of MgF_2 material are compared in terms of their densities, it is reported that the density of the *Pnnm* phase is 3.04 g/cm^3, while the *Imma 74* crystal structure is 1.87 g/cm^3(Material research, 2021). There is about a 38.49% difference in density between these two phases of MgF_2. Since we are interested in the modification of spectacle lenses, we focus on the optical properties of the *Imma 74* orthorhombic crystal structure with a density of 1.87 g/cm^3. Along with the optical properties, structural, mechanical, and electronic properties have also been calculated. In addition, by substituting Boron into the MgF_2 crystal structure and F-defect forming, we created the $MgF_{(2-x)}B_{(x)}$ (x=1.0) and MgF_1 (F-defect) phases, respectively, and calculated their physical properties. The reason for performing these doping and F-defect formation applications is to see the results of biocompatible doping such as Boron that can affect the mechanical properties of the material and to create a lighter coating material. The structural results of the formed MgF_1 and MgF_1B_1 phases are reported in Table 1. These results are the first in the literature.

In terms of their electronic and optical properties, it has been reported that the formation energy of the MgF_2 crystal structure occurred

Table 1
The calculated lattice parameters a(Å), b(Å), c(Å) and bulk modulus B_0(GPa) in the Boron-doped $MgF_{2-x}B_x$ (x=0.0 and 1.0) and F-defected MgF_1 compounds. The lattice symmetry is a conventional cell.

Structures	Method	Structural properties										
		a[Å]	b[Å]	c[Å]	α	β	γ	B_0[GPa]	Cell types	Crystal structures	Space G.	$Refs.$
MgF_2	Our Cal.	3.918	6.402	9.083	90.00	90.00	90.00	49.063	Conventional	Orthorhombic	Imma, 74	
	Our Cal.	5.891	5.891	5.891	141.16	114.18	79.14	49.063	Primitive	Orthorhombic	Imma, 74	
	Other Cal.	4.576 5.754 4.516	4.471 5.754 4.476	3.039 5.754 2.984	140.21	110.03	83.63	53.290	Primitive Primitive Primitive	Orthorhombic ($CaCl_2$)[a] Orthorhombic Orthorhombic ($CaCl_2$)[a]	Imma, 74 Pnnm	Arroussi and Ghezali (2018) Material research (2011) Haines et al. (2001)
	Exp.	4.516	4.476	2.984					Primitive	Orthorhombic ($CaCl_2$)[a]	Pnnm	Haines et al. (2001)
MgF_1B_1	Our Cal.	3.916	6.597	8.576	90.00	90.00	90.00	24.156	Conventional	Orthorhombic	Imma, 74	
MgF_1	Our Cal.	3.894	6.372	9.324	90.00	90.00	90.00	40.501	Conventional	Orthorhombic	Imma, 74	

[a]The crystal lattice of orthorhombic ($CaCl_2$) space groups is different from the orthorhombic $Imma$(74) group. They are listed in Table 1 for reference to previous studies. Tetragonal and cubic phases of the MgF_2 crystal structure were also studied. However, the densities of these phases are high (3.034–3.469 g/cm^3) for lenses. Besides, the density of the phase, which is the space group $Imma$(74), is more suitable for lenses (1.87 g/cm^3) than the others. This is the aim of our study. Our results are in good agreement with the ref (Material research, 2011). There are no previous experimental or theoretical studies for the $MgF_1B_1$and MgF_1 phases.

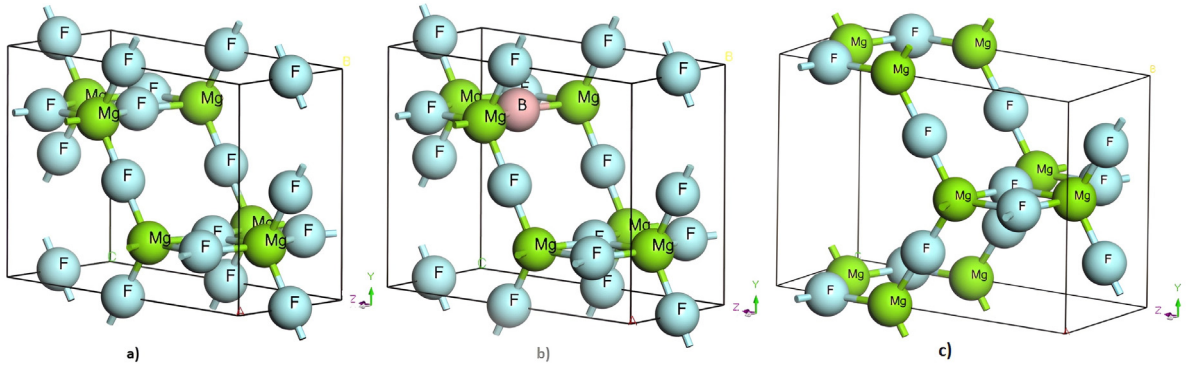

Fig. 1. The crystal structures of the (a) $MgF_{2-x}B_x$ (x=0), (b) Boron-doped $MgF_{2-x}B_x$ (x=1.0), and (c) F-defected MgF_1 compounds. The lattice symmetry is a conventional cell.

in the space group $Imma$ (74) is −3.73 eV and the bandgap is 6.47 eV (Material research, 2011). While the low formation energy $Imma$ *(74)* space group MgF_2 provides stability of the phase; The high bandgap supports the transparency of the compound in the UV and IR region. In light of all these reports, although there are crystal phases with other space symmetries of the MgF_2 crystal structure, it is clear that the MgF_2 phase occurred in the space group $Imma$ (74) would be a more suitable compound for spectacle lenses (Material research, 2011).

When our results in Table 1 are examined, under the $MgF_2 \rightarrow MgF_1B_1$ transformation, the lattice constants a and c decreased by approximately 0.05% and 5.58%, respectively, while the lattice constant b increased by 3.05%. However, when $MgF_2 \rightarrow MgF_1$ transformation is realized, the lattice constants a and b decrease by about 0.61% and 0.47%, respectively, while the constant c increases by 2.65%. In addition, the bulk modulus B (GPa) decreased very significantly by about 50.77% in the $MgF_2 \rightarrow MgF_1B_1$ transformation, but only by about 14.75% in the $MgF_2 \rightarrow MgF_1$ transformation.

The removal of an F atom from the MgF_2 lattice leads to the formation of an anion vacancy. This creates an excess of positive charge, thus increasing the electrostatic repulsive force between the positive charges in neighboring layers. This triggers an imbalance in the balance of forces in the lattice (Kittel, 1996). As a result, the surrounding anions relax and there is an expansion of the c-axis (9.324 Å). This is because the anions are now further apart to compensate for the new positive charge. The relaxation of the structure causes the binding energy between the atoms to decrease, resulting in a lower bulk modulus (B_0 = 40.501 GPa).

When MgF_2 is doped with a Boron atom, there is a change in the lattice structure that leads to a decrease in the bulk modulus. The comparative field strength of the B^{3+} cation plays an important role here, as it has a higher comparative field strength than Mg^{2+} and thus enters into a stronger electrostatic interaction with the anions. This leads to a compression of the c-axis (8.576 Å) and a significant decrease in the bulk modulus (B_0 = 24.156 GPa). The change in lattice parameters, which in turn affects the behavior of elastic properties.

The ionic charge and polarization also play an important role in the crystal chemical and physical explanation of these phenomena (Smart and Moore, 2005). In the case of vacancy formation due to the removal of a fluorine atom, an anion vacancy is formed, which leads to a higher polarization of the Mg^{2+} cation due to the high electronegativity of the fluorine. When MgF_2 is doped with Boron, the higher electronegative charge of Boron and its smaller size compared to Mg^{2+} leads to a higher ion polarization and a stronger force on the anions in the environment.

3.2. Mechanical properties

It is a good way to use elastic constants to obtain information about the mechanical behavior of materials. In particular, whether a crystal form is mechanically stable can be determined by calculating its elastic constants. Mathematically necessary and sufficient stability conditions for an orthorhombic crystal system to be mechanically stable can be

Table 2
The calculated elastic constants Cij(GPa) and polycrystalline aggregate properties of calculated bulk modulus B(GPa), Young's modulus E(GPa), Shear modulus G(GPa), Poisson's ratio ν, Micro-hardness H(GPa) and Pugh's ratio (G/B) in the polycrystalline Boron-doped $MgF_{2-x}B_x$ (x=0.0 and 1.0) and F-defected MgF_1compounds as Voigt, Reuss, and Hill respectively, compared with available experiment and previous theoretical studies.

Struc.	Met.	Polycrystalline aggregate properties [GPa]														Refs.
		B			E			G			ν					
		B_V	B_R	B_H	E_V	E_R	E_H	G_V	G_R	G_H	ν_V	ν_R	ν_H	H	G/B	
MgF_2	Our Cal.	50.617	47.509	49.063	52.419	35.908	44.282	19.745	13.067	16.406	0.327	0.374	0.3496	1.645	0.334	
	Other Cal.			53.290						22.310						Material research (2011)
MgF_1B_1	Our Cal.	27.742	20.570	24.156	26.799	17.812	22.313	10.007	6.570	8.288	0.339	0.356	0.346	0.792	0.343	
MgF_1	Our Cal.	40.990	40.011	40.501	33.526	25.308	29.491	12.293	9.074	10.683	0.364	0.395	0.379	0.864	0.264	
		Elastic constants C_{ij} [GPa]														
		C_{11}	C_{12}	C_{13}	C_{22}	C_{23}	C_{33}	C_{44}	C_{55}	C_{66}						
MgF_2	Our Cal.	104.751	25.220	30.374	82.087	52.453	52.819	16.717	27.474	10.631						
MgF_1B_1	Our Cal.	80.304	13.209	23.598	38.641	17.892	21.033	5.870	9.427	6.212						
MgF_1	Our Cal.	74.870	21.748	26.123	65.867	42.835	46.762	8.857	13.892	6.450						

listed as follows (Benckstein et al., 2001; Wallace, 1972; Mouhat and Coudert, 2014):

$$C_{11} > 0, C_{22} > 0, C_{33} > 0,\ C_{44} > 0, C_{55} > 0, C_{66} > 0. \quad (1)$$

$$C_{11} + C_{22} - 2C_{12} > 0. \quad (2)$$

$$C_{11} + C_{33} - 2C_{13} > 0. \quad (3)$$

$$C_{22} + C_{33} - 2C_{23} > 0. \quad (4)$$

$$C_{11} + C_{22} + C_{33} + 2C_{12} + 2C_{13} + 2C_{23} > 0. \quad (5)$$

$$\frac{1}{3}\left(C_{12} + C_{13} + C_{23}\right) < B < \frac{1}{3}\left(C_{11} + C_{22} + C_{33}\right). \quad (6)$$

The structural stability of the structures formed as a result of Boron doping, and mechanical stability are also important. In other words, to be able to say that the crystal phase is stable, the space symmetry of the crystal structure in which they are in equilibrium must meet all the mechanical stability conditions. All phases in our study came to equilibrium in the orthorhombic $Imma$ (74) space group. As given in Table 2, the calculated elastic constants C_{ij} of all phases are positive. Hence Eq. (1) is satisfied. Again, since the constants C_{11}, $C_{22,}$ and C_{33} are greater than the constants C_{12}, $C_{13,}$ and C_{23} in all phases, Eqs. (2), (3) and (4) are also satisfied. Since all elastic constants are positive, Eq. (5) is satisfied. If Table 2 is examined, it will be seen that Eq. (6) is satisfied for all phases. According to these results, all the studied phases fulfill all the mechanical stability conditions given for orthorhombic crystalline phases (Benckstein et al., 2001; Wallace, 1972). Thus, we can say that MgF_2, Boron doped $MgF_{2-x}B_x$ (x=1.0) and F-defected MgF_1 phases are both structurally and mechanically stable. The calculated elastic constants and polycrystalline aggregate properties for all phases are given in Table 2.

As given in Table 2, the bulk modulus B (GPa) value decreases from 49.063 GPa to 40.501 GPa (about 17.45%.) in the $MgF_2 \rightarrow MgF_1$ transformation is performed by creating the F-defect. This decrease indicates a softening in the crystal structure. When a thermal or mechanical shock is applied to the material, the probability of cracking is reduced. In the $MgF_2 \rightarrow MgF_1B_1$ transformation, a very high decrease of about 50.77% in the bulk modulus B (GPa) value was calculated. From this, it can be concluded that the MgF_1B_1 phase is extremely soft compared to the MgF_2 phase. Thus, a material that is more mechanically useful (less likely to crack) is obtained.

Shear modulus G (GPa) can be used to evaluate the flexibility of materials. As a result of our calculations, 34.88% and 40.48% decrease in shear modulus values were calculated for $MgF_2 \rightarrow MgF_1$ and $MgF_2 \rightarrow MgF_1B_1$ transformations, respectively. This decrease indicates that the flexibility of the phases increases.

In addition, Young's modulus E (GPa) value decreased by approximately 49.61% and 33.40%. The decrease in the value of this modulus indicates that the elasticity of the material increases (stiffness decreases). Thus, the elastic deformation that will occur as a result of the applied stress will be high. Increasing the elasticity of the material is a desirable property for spectacle lenses.

As the Poisson υ ratio increases, the plasticity of the material increases. The calculated Poisson υ ratios in all phases are between 0.34–0.38. These values show that the atoms forming the crystal structure are ionically bonded. Because, materials with a low Poisson υ ratio (υ = 0.1) have a covalent bonding force, while materials with a high Poisson υ ratio (υ = 0.25 or higher) have an ionic bonding force (Rahman et al., 2016a,b). The calculated Poisson υ ratios accurately are predicted the bonding structure (ionic) of the MgF_2, MgF_1B_1, and MgF_1 structures. Also, Poisson υ increases by approximately 8.36% in $MgF_2 \rightarrow MgF_1$ transformation. From this, it was determined the plasticity of the material has increased.

Pugh's ratio is defined as G/B. it is a simple indicator of the brittle–ductile characteristic of crystals (Pugh, 1954). Brittle materials have a ratio of $G/B > 0.5$, while ductile is less than 0.5 value (Rahman et al., 2016a,b). When Table 2 is examined, Pugh's ratios of MgF_2, MgF_1B_1, and MgF_1 phases were calculated as 0.334, 0.343, and 0.264, respectively. According to these results, it was determined that all studied phases had ductile mechanical behavior. Besides, the F-defected MgF_1 structure is about 21.11% ductile more than the other phases as it has a G/B ratio of 0.264. In other words, it is less fragile.

To evaluate the compressibility behavior of the material, the microhardness parameter H (GPa) was calculated with the following equation (Yousef et al., 2006).

$$H = \frac{(1 - 2\upsilon)\, E}{(1 + \upsilon) 6} \quad (7)$$

Finally, the Microhardness H (GPa) parameter is calculated to decrease by approximately 51.87% and 47.47% in the $MgF_2 \rightarrow MgF_1B_1$ and $MgF_2 \rightarrow MgF_1$ transformations, respectively. This decrease in H (GPa) indicates an increase in the compressibility or flexibility of the material. Conversely, it is an indicator of reduced fragility. Thus, reducing the possibility of micro-cracks in the material.

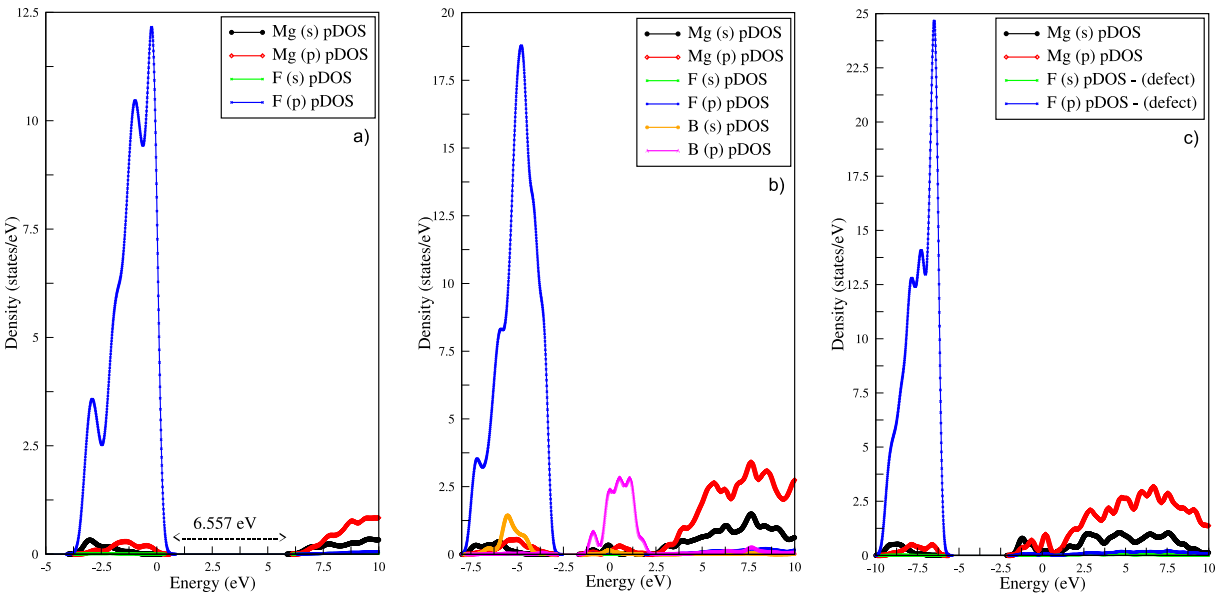

Fig. 2. The partial density of states for individual atoms of the (a) $MgF_{2-x}B_x$ (x=0), (b) Boron doped $MgF_{2-x}B_x$ (x=1.0), and (c) F-defected MgF_1 compounds. The Fermi level shifted to 0 eV.

3.3. Electronic properties

The density of state (DOS) and partial density of state (pDOS) calculations were made to determine the electronic behavior of the initial phase MgF_2, F-defected MgF_1, and Boron-doped MgF_1B_1 phases. Results obtained are presented in Figs. 2-(a), 2-(b), and 2-(c). If we focus on Fig. 2-(a), the electronic bandgap of the orthorhombic (*Imma 74*) MgF_2 crystal phase is calculated as 6.557 eV (the Fermi level shifted to 0 eV). This value indicates that the MgF_2 phase is a semiconductor. In addition, it is highly compatible with the electronic band gap value of the orthorhombic (*Imma 74*) MgF_2 phase reported as 6.47 eV in previous studies (Material research, 2011). The MgF_2 phase has an electronic bandgap of 6.557 eV, making the crystal phase almost an insulating semiconductor. This high band gap value supports the transparency of the MgF_2 crystalline phase. In other words, when used as a coating in the form of spectacle lenses or thin films (thickness is very important for the reflective or antireflective behavior of the coating), it will reduce the reflections that will occur on the surfaces and ensure that the lens exhibits a physical behavior in a direction that will increase the light transmittance.

Here, as given in Fig. 2-(a) is examined, according to the pDOS distributions, it is seen that extremely high contributions come from the p orbitals of F atoms to the valence band. In addition, also the contributions from the s and p orbitals of Mg atoms and the s orbitals of F atoms are extremely low. These results show that the p orbitals of F atoms have a great influence on both the structural and mechanical stability of the orthorhombic (*Imma 74*) MgF_2 crystal phase. This states that it can be interpreted that a significant change in the physical behavior of the crystal phase will not occur when a change is made in the form of a defect or substitution on the Mg atoms. On the contrary, it also indicates that if the defect or substitution process is done with F atoms, serious physical behavior changes can be realized in the crystal structure. Figs. 2-(b) and 2-(c) are examined, and the accuracy of our claim can be easily seen. In addition, again when focusing on Fig. 2-(a), it is seen that the contribution from the p orbitals of Mg atoms is high in the conduction band. Therefore, the p orbitals of Mg atoms play as much of a role as the p orbitals of F atoms in the transparency or light transmittance of the MgF_2 crystal phase.

The DOS and pDOS distributions of the $MgF_{2-x}B_x$ (x=1.0) doped crystal phase formed by the substitution of Boron to the orthorhombic (*Imma 74*) MgF_2 crystal phase, It is given in Fig. 2-(b). As seen in Fig. 2-(b), the p orbitals of the F atoms are again quite dominant in the lower parts of the Fermi level (at 0 eV). In the upper parts of the Fermi level, the p orbitals of Mg atoms dominate. The distribution here is it is very similar to the distribution in Fig. 2-(a). However, when Boron was substituted to the MgF_2 crystal phase, the contributions from the p orbitals of the B atoms spread around the Fermi level (at 0 eV). Since this behavior fills the band gap around the Fermi level of the crystal, $MgF_{2-x}B_x$ (x=1.0) has a metallic (conductive) nature. This indicates that the $MgF_{2-x}B_x$ (x=1.0) crystal phase has an opaque structure. That is, it is not correct to produce a bulky spectacle lens from this phase. However, this result also shows that the $MgF_{2-x}B_x$ (x=1.0) crystalline phase can be used quite efficiently as both an anti-reflective and a mirror coating depending on the coating thickness.

The electronic behavior of the MgF_1 crystal structure in which the F defect is formed in the MgF_2 crystal is given in Fig. 2-(c). The decrease of the F atom in the crystal structure resulted in the transformation of the MgF_2 phase, which is a semiconductor, into a metallic character. In the MgF_2 crystal, As seen in Fig. 2-(a), when the contribution of F atoms forming the uppermost levels of the valence band decreased, the p orbital states of Mg atoms, which have a say in the conduction band above the Fermi level, spread towards the Fermi level. As a result of this behavior, the transformation from semiconductor to conductivity was realized by filling the electronic bandgap. As a result, the metallic nature of the MgF_1 phase, as in the $MgF_{2-x}B_x$ (x=1.0) phase, can be efficiently exploited by thickness optimization in spectacle lens coatings. When metals are considered in bulk, they have an opaque nature. However, they can transmit light when they are around 0.1 μm (about 100 nm) thick. When optimized in this way, they can be used as anti-reflection or mirror coating.

3.4. Optical properties

The data obtained from the calculations to analyze the optical properties of $MgF_{2-x}B_x$ (x=0.0 and 1.0) and MgF_1 crystal phases are presented in Figs. 3-(a), 3-(b), 3-(c), 3-(d), and 3-(e). However, for our study, we made our evaluations in the lower (380 nm), average (580 nm), and upper limit (780 nm) range of the visible region, respectively. Outside these limits, pre-measured or calculated results are available for the ultraviolet (UV) and infrared (IR) regions related to the MgF_2 crystal structure (Babu et al., 2011; Wang et al., 2013; Arroussi and Ghezali, 2018). However, we did not report them in Tables 3 and 4

Table 3
The calculated Refractive index ($N = n + ik$), Refractive index norm ($|N|$), and Reflection coefficient (R) for the Boron-doped $MgF_{2-x}B_x$ (x=0.0 and 1.0) and F-defected MgF_1 compounds.

Structures	Method	Index	Refractive index ($N = n + ik$)			Refractive index norm ($|N|$)			Reflection coefficient (R)		
			Wavelength (nm)			Wavelength (nm)			Wavelength (nm)		
			380	580	780	380	580	780	380	580	780
MgF_2	Our Cal.	n	1.264	1.231	1.228	1.264	1.231	1.228	0.014	0.011	0.011
	Our Cal.	k	0.000	0.000	0.000						
MgF_1B_1	Our Cal.	n	1.319	1.086	0.701	1.321	1.086	0.749	0.020	0.002	0.053
	Our Cal.	k	0.077	0.023	0.262						
MgF_1	Our Cal.	n	1.144	1.626	1.613	1.221	1.656	1.615	0.042	0.070	0.056
	Our Cal.	k	0.427	0.314	0.087						

Table 4
The calculated Reflectance percentage (P), Total reflected light percentage, and Total transmitted light percentage for the Boron-doped $MgF_{2-x}B_x$ (x=0.0 and 1.0) and F-defected MgF_1 compounds.

Struc.	Meth.	Index	Refractive index ($N = n + ik$)			Reflectance percentage (P) Single layer/ front side			Reflectance percentage (P) Single layer/ back side			Total reflected light Percentage			Total transmitted light percentage		
			Wavelength (nm)			Wavelength (nm)			Wavelength (nm)			Wavelength (nm)			Wavelength (nm)		
			380	580	780	380	580	780	380	580	780	380	580	780	380	580	780
MgF_2	Our Cal.	n	1.264	1.231	1.228	1.264	1.231	1.228	0.014	0.011	0.011	2.699	2.137	2.114	97.30	97.86	97.89
	Our Cal.	k	0.000	0.000	0.000												
MgF_1B_1	Our Cal.	n	1.319	1.086	0.701	1.321	1.086	0.749	0.020	0.002	0.053	3.784	0.341	5.851	96.22	99.66	95.91
	Our Cal.	k	0.077	0.023	0.262												
MgF_1	Our Cal.	n	1.144	1.626	1.613	1.221	1.656	1.615	0.042	0.070	0.056	1.970	11.814	10.755	98.03	88.19	89.25
	Our Cal.	k	0.427	0.314	0.087												

as they are not in the target wavelength regions (380 nm to 780 nm). The change of refractive indices of $MgF_{2-x}B_x$ (x=0.0 and 1.0) and MgF_1 crystal phases according to wavelength is given in Fig. 3-(a). If we focus on Fig. 3-(a), the real part (n) of the refractive index of the MgF_2 phase in the visible region has values between 1.264 and 1.228. The imaginary (k) part is zero. Accordingly, the refractive index N consists of completely real (n) parts.

Here, the norm of the refractive index |N| is calculated from the following equation:

$$|N| = \sqrt{n^2 + k^2} \tag{8}$$

Similarly, the reflection coefficient R;

$$R = \frac{(n-1)^2 + k^2}{R = (n+1)^2 + k2} \tag{9}$$

calculated from Eq. (9). Finally, the percent reflection rate P,

$$P = \frac{(n_j - n_i)^2}{(n_j + n_i)^2}(I_p) \tag{10}$$

calculated from Eq. (10). Where n_j is the refractive index of the lens (or coating); n_i is the refractive index of the air (or the medium in which the lens is located); I_p is the original light ratio.

In the Boron substituted MgF_1B_1 phase, it was determined that the real part of the refractive index n value increased by approximately 4.32% in the lower parts of the visible light (≅ 380 nm). In addition, an increase in the imaginary part (k) values of approximately 7% below the visible region (≅ 380 nm) and approximately 26.18% above (≅ 780 nm) was calculated. Based on these results, the norm of the refractive index is |N| although it increased by about 4.5% in the lower part of the visible region, a decrease of approximately 11.75% and 39.05% was determined in the middle and upper regions, respectively.

In the F-defected MgF_1 phase, a satisfactory increase of approximately 32.015% and 31.31% was detected in the real (n) part of the refractive index in the middle (580 nm) and upper (780 nm) visible light regions, respectively. The norm of the refractive index |N| of this phase was calculated as 1.221, 1.656, and 1.615, respectively in the lower (380 nm), middle (580 nm), and upper (780 nm) visible regions. In the results obtained, it is seen that the highest refractive index ($|N|$) and reflection coefficient (R) are found in the F-defected MgF_1 phase.

Focusing on Table 4, in the $MgF_2 \rightarrow MgF_1B_1$ transformation, the light transmission rate of the layer decreased from 97.30% to 96.22% in the lower region of visible light; increased from 97.86% to 99.66% in the middle region; In the upper region, it was calculated that it decreased from 97.89% to 95.91%. These results show that the light transmittance (or reflection rate) can be optimized around 10% by adding F-defected or Boron to the MgF_2 crystal. We think that our results will contribute to the literature on industrial glass (lens), spectacle lens, or layer applications.

As given in Fig. 3-(b), it has been determined that a high absorption occurs in the range of about 20 nm–200 nm in small wavelength (or high energy) in all phases. This behavior is quite satisfactory in terms of UV filtration. However, according to MgF_2 absorption slightly decreases in MgF_1 and MgF_1B_1 phases, respectively. On the contrary, no absorption occurs in the visible light region (380 nm–780 nm), especially in the MgF_2 and MgF_1B_1 phases. This behavior is pleasing as it supports the lossless passage of incident light through the lens or layer.

However, in the MgF_1 phase, a relatively small amount of absorption occurs in the lower regions of visible light in the range of about 380 nm to 475 nm compared to the UV region. Although this reduces the amount of incoming light, it can create an advantage in practice. Because, as is known, digital displays produce a high proportion of blue-violet light, known as artificial blue high-energy visible light (HEV-light, 400–450 nm). This light passes through the eye and reaches

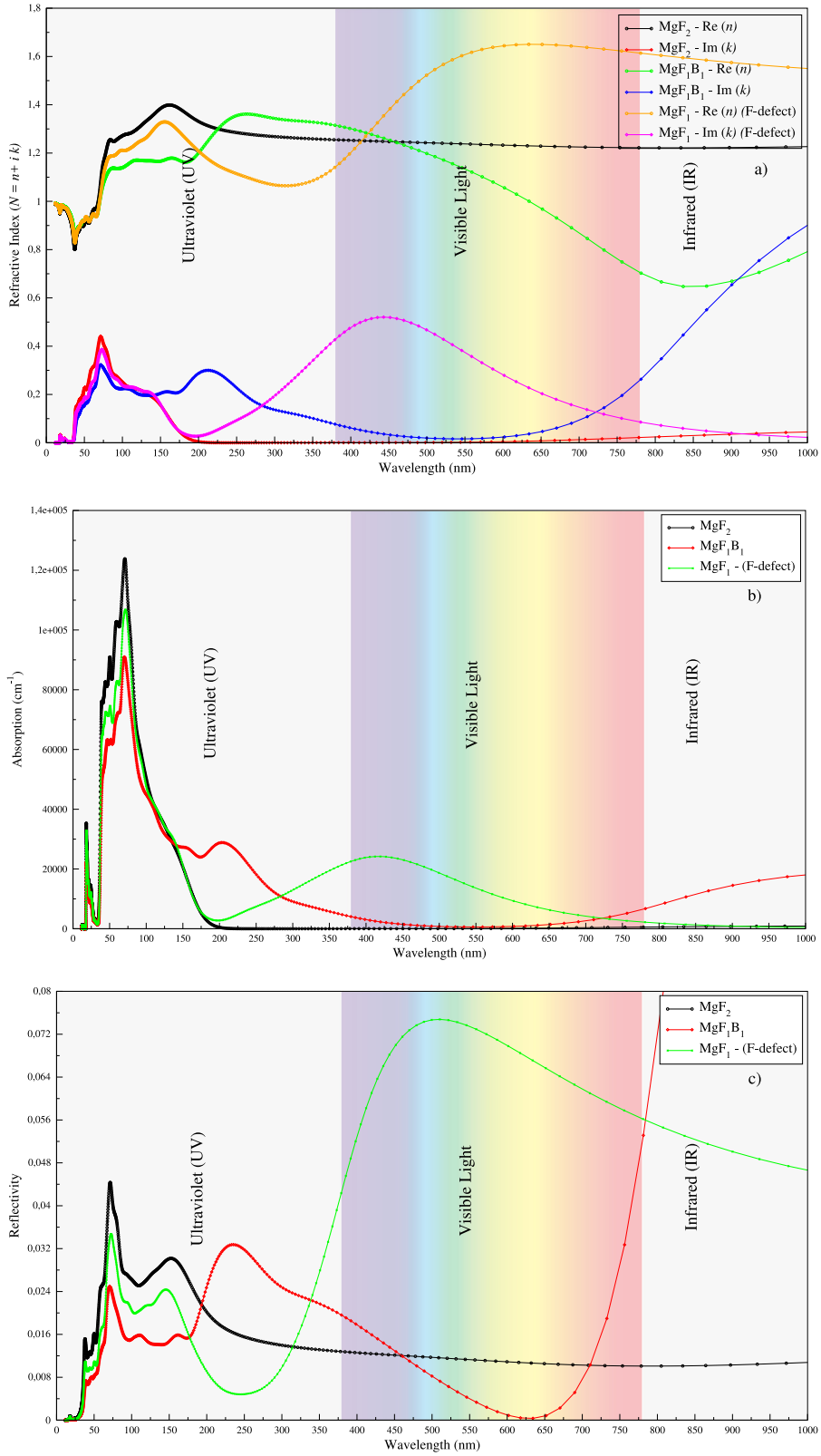

Fig. 3. The optical functions (a) Refractive index, (b) Absorption, (c) Reflectivity, (d) Dielectric function, and (e) Loss function of the (a) $MgF_{2-x}B_x$ (x=0), (b) Boron doped $MgF_{2-x}B_x$ (x=1.0), and (c) F-defected MgF_1 compounds. The calculations are for polycrystalline form.

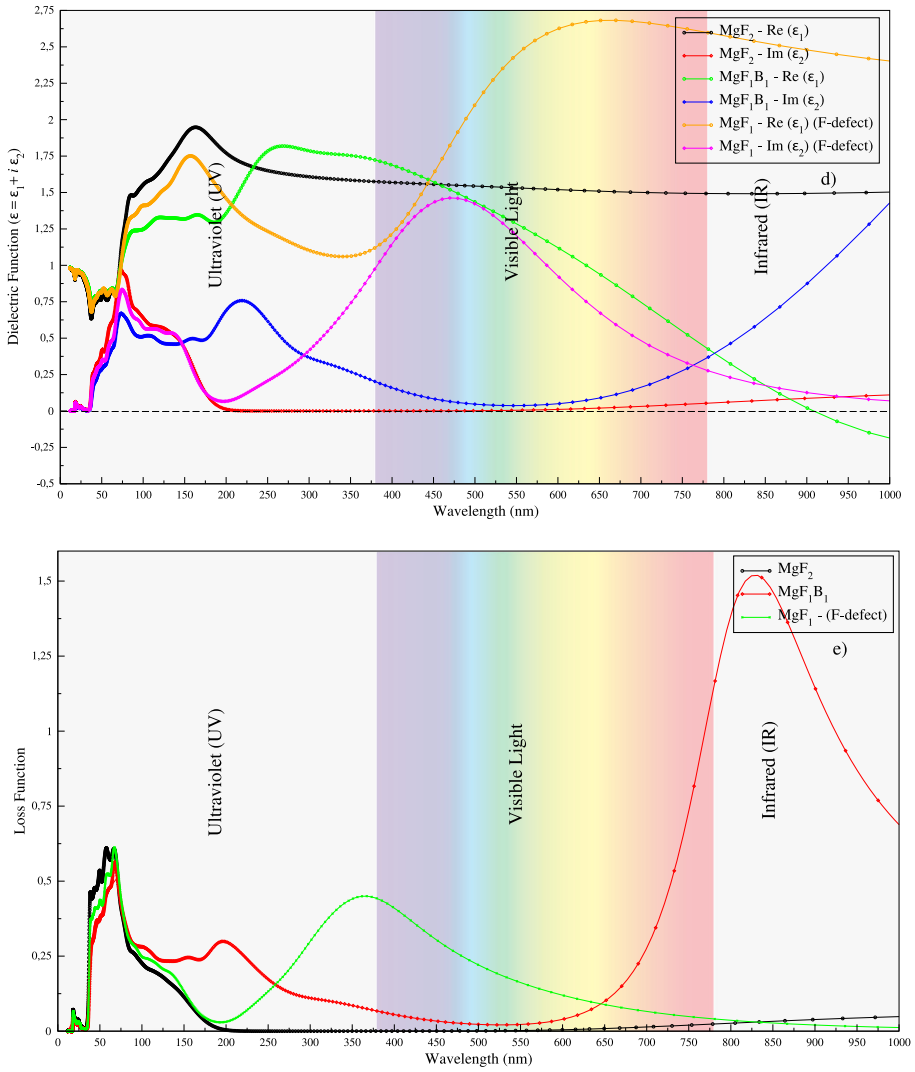

Fig. 3. (*continued*).

the retina without being filtered (absorbed). Over long periods, it causes permanent damage to the retina. If paying attention to Fig. 3-(b), it was determined that the MgF_1 phase had moderate absorption in the 400–450 nm range. This behavior shows that this phase can be used as an efficient filter (absorber) for HEV-light radiations.

Reflectance behaviors of MgF_2, MgF_1B_1, and MgF_1 phases are given in Fig. 3-(c). If Fig. 3-(c) is examined, it has good anti-reflection characteristics up to about 27 nm (≅ 45 eV) in all phases. Because of this nature, they can be good anti-reflection coating candidates. These results are in good agreement with previous studies (Babu et al., 2011). In addition, the highest reflectivity between 50 nm and 75 nm is in MgF_2, MgF_1, and MgF_1B_1 phases, respectively. This region is the high-energy vacuum UV radiation region and the reflectivity of the coating is very important.

Similarly, the MgF_1B_1 phase is highly reflective compared to other phases in the 200 nm to 350 nm range. This region is relatively low in energy but still harmful to the eye. Also, the MgF_1B_1 phase has very good anti-reflection behavior in the approximately mid-visible (580–675 nm) region. In contrast, the MgF_1 phase gives a very high reflection peak in the HEV-light radiation (400–450 nm) and blue color (475–525 nm) regions. This behavior, when considered together with the absorption behavior of the MgF_1 phase, is proof that it has a very good reflective (or filtering) potential. In addition, MgF_2 and MgF_1 phases exhibit anti-reflection behavior in the IR region, while the MgF_1B_1 phase has a very good reflective coating potential in the entire IR region after approximately 800 nm.

The optical behavior of a medium interacting with light for different photon energies is described by the complex dielectric function ($\varepsilon = \varepsilon_1 + i\varepsilon_2$). The peak value of the real (ε_1) part of the complex dielectric function is associated with electron excitation. Using the elements of the momentum matrix formed by the occupied and unoccupied states, the imaginary (ε_2) part of the complex dielectric function can be calculated. Also, the real (ε_1) part can be derived from the imaginary (ε_2) part by using the Kramer-Kronig relation. Also, the real (ε_1) part of the complex dielectric function (ε) exhibits dispersive behavior, and the imaginary (ε_2) part exhibits absorptive behavior. Both components as a function of wavelength (nm) are given in Fig. 3-(d). On focus Fig. 3-(d), for the MgF_2 phase, the highest peak of the imaginary (ε_2) part in the UV region in the range of about 30 nm–75 nm corresponds to the wavelength value of 72 nm (≅ 17–20 eV). Other peaks were localized at 60, 50, 44, and 38 nm, respectively. The imaginary (ε_2) part behavior of the MgF_1B_1 and MgF_1 phases is similar to that of the MgF_2 phase. In addition, we calculated the $\varepsilon_1(0)$ value of the real part of the complex dielectric function as 1.97. These calculated peaks are quite compatible with other theoretical and experimental studies and are proof of the consistency of our calculations (Babu et al., 2011; Williams et al., 1967).

The energy loss function can also be derived from the imaginary part (ε_2) of the reciprocal of the complex dielectric function (ε). This function determines the energy loss of a fast electron traveling through a material. The Loss Function distributions of MgF_2, MgF_1B_1, and

MgF_1 phases depending on wavelength (nm) are given in Fig. 3-(e). The Loss function peak for the MgF_2 phase occurs at a wavelength of approximately 56 nm. This obtained result is consistent with the experimentally measured result of 24.5 eV (≅50.61 nm) (Williams et al., 1967). Again, it is quite close to the theoretically calculated value of 26 eV (Babu et al., 2011). In this respect, the calculated loss Function distribution for the MgF_2 phase is consistent with other studies. In addition, the peak values of the loss functions of the MgF_1B_1 and MgF_1 phases correspond to wavelengths of 66 nm (18.78 eV) and 67 nm (18.5 eV), respectively. In addition, the loss function peaks were calculated for the MgF_1B_1 phase at wavelengths of 196 nm (6.32 eV) and 828 nm (1.499 eV), respectively. Finally, a peak corresponding to the wavelength of 361 nm (3.43 eV) of the MgF_1 phase was determined. There is no previous study with which we can compare these results. Therefore, we think that our results will contribute to the literature.

4. Conclusions

This study shows that when an F atom is removed from MgF_2, the electrostatic repulsion force increases due to the anion vacancy and the interatomic binding energy weakens and the surrounding anions relax (c=9.324 Å). This is the reason for the approximately 17.45% decrease in the bulk modulus *B* (GPa) value. On the contrary, it determined that when boron is added, the higher electronegative charge of boron and its smaller size compared to Mg cause a higher ion polarization and a stronger force on the anions in the medium, resulting in a compression of the *c*-axis (8.576 Å) and the bulk modulus *B* (GPa) is reduced by about 50.77%.

Since the values of Bulk modulus *B* (GPa), Shear modulus *G* (GPa), Young's modulus *E (GPa)*, and micro-hardness *H* (GPa) decrease in $MgF_2 \rightarrow MgF_1B_1$ transformation, it is determined that the cracking, rupture, stiffness and micro-crack formation status of the material decreases respectively. The plasticity of the MgF_1 phase is higher than that of MgF_2 and since the Pugh ratio (G/B) is calculated as 0.264, it is determined that it has the highest ductility.

It has been calculated that the MgF_2 phase has an electronic bandgap of approximately 6.557 eV. It was determined that the contributions from the p orbitals of the F atoms to the valence region were very high compared to the Mg atoms. When Boron is substituted, contributions from the p orbitals of B atoms are calculated to diffuse around the Fermi level (at 0 eV). Therefore, the MgF_1B_1 phase is metalized. Due to this metallization, it is determined that MgF_1B_1 and MgF_1 phases will be more resistant to cracking, fracture, and scratching under thermal or mechanical shock conditions.

The MgF_1B_1 phase was calculated to have a good UV filtration property in terms of light transmission. The MgF_1 phase is found to be slightly absorptive in the range of about 380–475 nm and reflective in the range of 200–350 nm. Hence, it can be used as a good HEV-light (400–450 nm) radiation absorber and mirror coating, respectively.

Declaration of competing interest

The authors declare that they have no known competing financial interests or personal relationships that could have appeared to influence the work reported in this paper.

Data availability

The data that has been used is confidential.

Acknowledgments

The authors would like to thank M. Adlung-Baykara, evo-Silicatforschung, Germany, for discussions of the results and critical reading of this work.

Appendix A. Supplementary data

Supplementary material related to this article can be found online at https://doi.org/10.1016/j.rsurfi.2023.100126.

References

Arroussi, A., Ghezali, M., 2018. First-principles study of the structural electronic and optical properties of MgF_2. Optik 164, 16–27.
Babu, K.R., Lingam, C.B., Auluck, S., Tewari, S.P., Vaitheeswaran, G., 2011. Structural thermodynamic and optical properties of MgF_2 studied from first-principles theory. J. Sol. State Chem. 184 (2), 343–350.
Benckstein, O., Klepeis, J.E., Hart, G.L.W., Pankratov, O., 2001. First-principles elastic constants and electronic structure of α-Pt2Si and PtSi. Phys. Rev. B 63, 134112.
Clark, S.J., Segall, M.D., Pickard, C.J., Hasnip, P.J., Probert, M.J., Refson, K., Payne, M.C., 2005. First principles methods using CASTEP. Z. Kristallographie 220 (5–6), 567–570.
Duyar, O., Durusoy, H.Z., 2004. Design and preparation of antireflection and reflection optical coatings. Turk. J. Phys. 28, 139–144.
Fischer, T.H., Almlof, J., 1992. General methods for geometry and wave function optimization. J. Phys. Chem. 96 (24), 9768–9774.
Goldschmidt, V.M., 1926. Die Gesetze der Krystallochemie. Naturwissenschaften 14, 477–485.
Haines, J., Leger, J.M., Gorelli, F., Klug, D.D., Tse, J.S., Li, Z.Q., 2001. X-ray diffraction and theoretical studies of the high-pressure structures and phase transitions in magnesium fluoride. Phys. Rev. B 64, 134110.
Helvacı, C., 2017. Borate deposits: An overview and future forecast with regard to mineral deposits. J. Boron 2, 59–70.
Kitamura, Y., Miyazaki, N., Mabuchi, T., Nawata, T., 2009. Birefringence simulation of annealed ingot of magnesium fluoride single crystal. J. Cryst. Growth 311.
Kittel, C., 1996. Introduction to Solid State Physics, 7th Edition Oldenverlag, pp. 584–588.
Korkmaz, S., Elmas, S., Ekem, N., Pat, S., Balbağ, M.Z., 2012. Deposition of MgF2 thin films for antireflection coating by using thermionic vacuum arc (TVA). Opt. Commun. 285, 2373–2376.
Kresse, G., Furthmuller, J., 1996a. Efficiency of ab-initio total-energy calculations for metals and semiconductors using a plane-wave basis set. Com. Mater. Sci. 6, 15–50.
Kresse, G., Furthmuller, J., 1996b. Efficient iterative schemes for ab-initio total-energy calculations using a plane-wave basis set. Phys. Rev. B 54 (11169).
Kresse, G., Hafner, J., 1994. Norm-conserving and ultrasoft pseudopotentials for first-row and transition elements. J. Phy. Condens. Matt. 6 (8245).
Material research, 2011. Material phases reports for the material properties. https://materialsproject.org/materials/mp-1180279/#corrections-eqn. (Accessed 10 2023).
Material research, 2021. Material phases reports for the mgf_2 phase properties. https://materialsproject.org/materials?chemsys=Mg-F. (Accessed 15 2023).
Monkhorst, H.J., Pack, J.D., 1976. Special points for Brillouin-zone integrations. Phys. Rev. B 13, 5188–5192.
Mouhat, F., Coudert, F.X., 2014. Necessary and sufficient elastic stability conditions in various crystal systems. Phys. Rev. B 90, 224104.
Perdew, J.P., Burke, K., Ernzerhof, M., 1996. Generalized gradient approximation made simple. Phys. Rev. Lett. 77 (3865).
Pugh, S., 1954. XCII relations between the elastic moduli and the plastic properties of polycrystalline pure metals. London Edinburgh Philos. Mag. J. Sci. London, Edinburgh Dublin Philos. Mag. J. Sci 45, 823–843.
Rahman, M.A., Rahaman, M.Z., Rahman, M.A., 2016a. The structural elastic, electronic and optical properties of MgCu under pressure: A first-principles study. Int. J. Mod. Phys. B 30, 1650199.
Rahman, M.A., Rahman, M.Z., Sarker, M.A.R., 2016b. First-principles investigation of structural elastic, electronic, and optical properties of $HgGeB_2$ (B=P, As) chalcopyrite semiconductors. Com. Condens. Matter. 9, 19–26.
Sandu, A.V., Baltatu, M.S., Nabialek, M., Savin, A., Vizureanu, P., 2019. Characterization and mechanical proprieties of new TiMo alloys used for medical applications. Materials 12 (18), 2973.
Smart, L.E., Moore, E.A., 2005. Solid State Chemistry, 3th Edition Boca Raton, pp. 188–262.
Thielsch, R., Meiling, W., 1990. Structural optical and electronical properties of mixed dielectric films. Vacuum 41 (4–6), 1147–1150.
Wallace, D.C., 1972. Thermodynamics of Crystals. Wiley, New York, Chap. 1.
Wang, L.P., Han, P., Zhang, Z., Zhang, C., Xu, B., 2013. Effects of thickness on the structural electronic, and optical properties of MgF_2 thin films: The first-principles study. Com. Mat. Sci. 77, 281–285.
Williams, M.W., Macrae, R.A., Arakawa, E.T., 1967. Optical properties of magnesium fluoride in the vacuum ultraviolet. J. Appl. Phys. 38 (4), 1701–1705.
Wojciechowska, M., Zielinski, M., Pietrowski, M., 2003. MgF_2 as a non-conventional catalyst support. J. Fluorine Chem. 120 (1), 1–11.
Yousef, E.S., El-Adawy, A., El-KheshKhany, N., 2006. Effect of rare earth (Pr_2O_3 Nd_2O_3, Sm_2O_3, Eu_2O_3, Gd_2O_3, and Er_2O_3) on the acoustic properties of glass belonging to bismuth–borate system. Solid State Commun. 139, 108–113.